

FocusDPO: Dynamic Preference Optimization for Multi-Subject Personalized Image Generation via Adaptive Focus

Qiaoqiao Jin*, Siming Fu^{*†}, Dong She*, Weinan Jia, Hualiang Wang, Mu Liu, Jidong Jiang[‡]

ByteDance FanQie

*Equal Contribution, [†]Project Lead, [‡]Corresponding Author

Abstract

Multi-subject personalized image generation aims to synthesize customized images containing multiple specified subjects without requiring test-time optimization. However, achieving fine-grained independent control over multiple subjects remains challenging due to difficulties in preserving subject fidelity and preventing cross-subject attribute leakage. We present **FocusDPO**, a framework that adaptively identifies focus regions based on dynamic semantic correspondence and supervision image complexity. During training, our method progressively adjusts these focal areas across noise timesteps, implementing a weighted strategy that rewards information-rich patches while penalizing regions with low prediction confidence. The framework dynamically adjusts focus allocation during the DPO process according to the semantic complexity of reference images and establishes robust correspondence mappings between generated and reference subjects. Extensive experiments demonstrate that our method substantially enhances the performance of existing pre-trained personalized generation models, achieving state-of-the-art results on both single-subject and multi-subject personalized image synthesis benchmarks. Our method effectively mitigates attribute leakage while preserving superior subject fidelity across diverse generation scenarios, advancing the frontier of controllable multi-subject image synthesis.

Page: <https://bytedance-fanqie-ai.github.io/FocusDPO/>

1 Introduction

The rapid advancement of diffusion models [9] has revolutionized personalized image generation [4, 5, 8, 10, 19, 32, 37, 39, 40], enabling the synthesis of high-quality images featuring specific subjects of interest. Among various personalization paradigms, multi-subject personalized image generation has emerged as a particularly compelling research direction, aiming to synthesize customized images containing multiple specified subjects without requiring computationally expensive test-time optimization. This capability holds significant practical value for applications ranging from creative content generation to personalized advertising and digital art creation.

The multi-subject personalization methods [4, 12, 16, 22, 23, 37–39] fundamental difficulty lies in achieving fine-grained independent control over multiple subjects while simultaneously preserving the visual fidelity of each individual subject. Existing approaches [37–39] often struggle with cross-subject attribute confusion,



Figure 1 Our proposed FocusDPO demonstrates capabilities in single-subject and multi-subject driven generation tasks.

where characteristics from one subject inadvertently influence the appearance of another, leading to inconsistent or corrupted generations. Moreover, maintaining the precise details and distinctive features of each reference subject becomes increasingly complex as the number of subjects grows, particularly when subjects share similar semantic categories or visual attributes.

Recent efforts in multi-subject generation have explored various strategies, such as PatchDPO [13], it estimates the quality of image patches within each generated image and accordingly trains the model. However, these methods [13, 34] typically employ fixed treatment on different image regions across different training timesteps, failing to account for the varying complexity and semantic importance of different areas within the generated image. This limitation becomes particularly pronounced when dealing with subjects of different scales, positions, or semantic complexity levels. As shown in Fig. 2, when the noise strength is changed, the regions that require focused attention during model training should adapt accordingly. At higher noise levels, the model needs to concentrate on global structure and semantic features, while at lower noise levels, attention should shift toward fine-grained details and local texture preservation. **This observation motivates our dynamic focus modulation mechanism, which adjusts the spatial focus regions based on the current denoising step and the complexity of the supervision signal.**

To address these challenges, we present FocusDPO, a novel framework that leverages dynamic Direct Preference Optimization to achieve superior multi-subject personalized image generation. Our **key insight** is that effective multi-subject control requires adaptive attention allocation based on both the dynamic correspondence between generated and reference subjects and the semantic complexity of supervision images. Rather than applying uniform optimization pressure across all image regions, FocusDPO intelligently identifies regions of focus and adjusts the training dynamics accordingly. The core contribution of our approach lies in its weighted training strategy that rewards high-quality image patches while penalizing regions with low prediction confidence. This selective optimization enables the model to concentrate computational resources on challenging areas while maintaining efficiency in well-handled regions. Furthermore, our framework establishes robust correspondence mappings between generated and reference subjects, ensuring consistent identity preservation across diverse generation scenarios. Extensive experiments demonstrate that FocusDPO

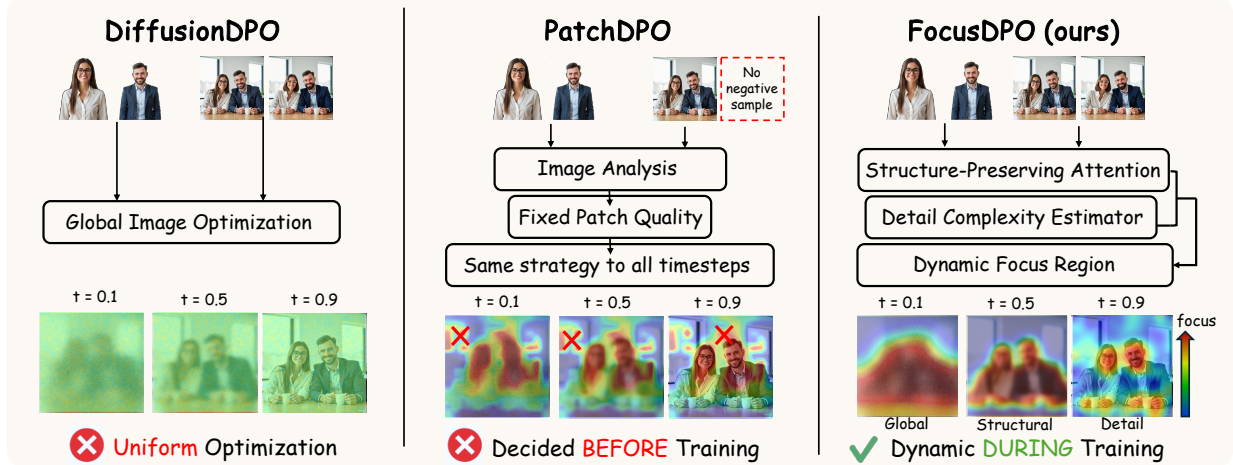


Figure 2 Comparison of training optimization strategy: DiffusionDPO’s uniform optimization (left) vs. PatchDPO’s fixed patch optimization (middle) vs. FocusDPO’s adaptive focus strategy (right).

substantially enhances the performance of existing pre-trained personalized generation models, achieving state-of-the-art results on both single-subject and multi-subject personalized image synthesis benchmarks. The proposed framework effectively addresses attribute leakage while maintaining superior subject preservation, marking a significant step forward in controllable image generation. Our primary contributions are threefold:

- We introduce FocusDPO, which intelligently identifies “focus regions” characterized by high semantic complexity and detailed-preserving generation difficulty. By adaptively intensifying optimization on these key areas, it efficiently enhances overall image quality and training stability.
- By dynamic semantic and detail-preserving preference optimization, our method effectively mitigates identity confusion and attribute leakage in multi-subject scenarios, ensuring faithful subject preservation.
- Extensive experiments demonstrate that FocusDPO substantially boosts the performance of existing models, achieving state-of-the-art results on both single- and multi-subject personalized image synthesis benchmarks.

2 Related Work

2.1 Subject-driven Generation

Multi-subject personalized generation extends beyond single-subject methods like DreamBooth [32] and Textual Inversion [8], presenting significant challenges in maintaining subject integrity while preventing inter-subject interference. Recent approaches have explored various architectural strategies: OmniControl [39] and IC LoRA [11] leverages DiTs as image encoders for subject references, while MS-Diffusion [35] and MIP-Adapter [14] introduce specialized adapters for multiple subjects. UNO [37] employs progressive training with Universal Rotary Position Embedding to mitigate attribute confusion, and XVerse [4] utilizes text-stream modulation for reference image processing. Despite these advances, existing methods struggle with inter-subject entanglement and attribute leakage, particularly when subjects share similar visual characteristics. This work addresses these limitations through dynamic semantic guidance, achieving robust multi-subject generation with enhanced semantic consistency.

2.2 Diffusion-based Preference Optimization

Direct Preference Optimization (DPO) [29, 41, 43] and Reinforcement Learning from Human Feedback (RLHF) [1, 3, 7, 18], originally formulated for language model alignment, have been successfully adapted to diffusion-based image synthesis through methods including DPOK [7], DDPO [2], DRaFT [6] and AlignProp [27] for enhancing generation quality. However, standard DPO frameworks fall

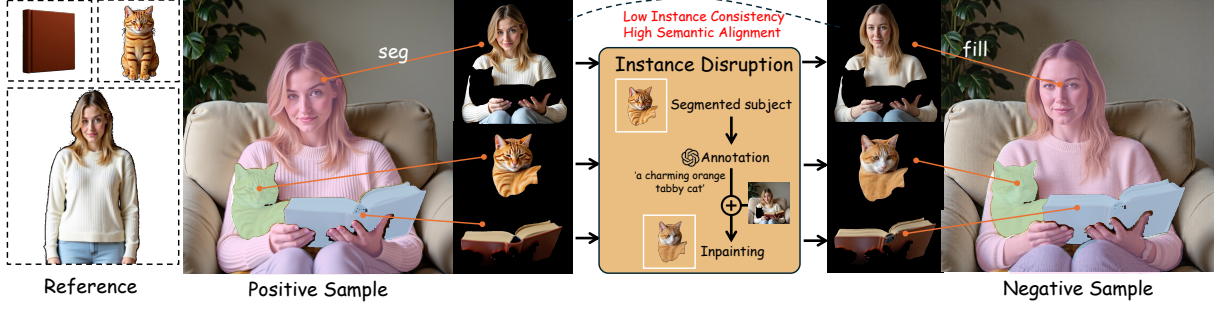


Figure 3 Disrupted-Instance Pair Dataset (DIP) dataset construction workflow. Preference pairs are generated by creating subject-consistent images, then introducing controlled perturbations to segmented areas to produce degraded counterparts.

short in consistency-sensitive tasks due to semantic confounds in global image comparisons. PatchDPO [13] mitigates this by optimizing preferences at the patch level, promoting finer-grained consistency learning. Unlike PatchDPO, which relies on static supervision without explicit positive-negative pairs, our method builds semantically aligned pairs and employs dynamic objectives to better preserve consistency.

3 Preliminary: Diffusion-DPO

Our work builds upon Diffusion Direct Preference Optimization (Diffusion-DPO) [34], a powerful framework for aligning text-to-image diffusion models with human preferences without requiring an explicit reward model. The training data for this process consists of preference pairs $\mathcal{D} = \{(x_0^w, x_0^l)\}$, where x_0^w is the preferred (winning) image and x_0^l is the dispreferred (losing) image for a given prompt. The core idea of Diffusion-DPO is to reinterpret the DPO loss in the context of diffusion model training:

$$\mathcal{L}(\theta) = -\mathbb{E}_{(x_0^w, x_0^l) \sim \mathcal{D}, t \sim \mathcal{U}(0, T), x_t^w \sim q(x_t^w | x_0^w), x_t^l \sim q(x_t^l | x_0^l)} \log \sigma(-\beta T \omega(\lambda_t) (\|\epsilon^w - \epsilon_\theta(x_t^w, t)\|_2^2 - \|\epsilon^w - \epsilon_{\text{ref}}(x_t^w, t)\|_2^2 - (\|\epsilon^l - \epsilon_\theta(x_t^l, t)\|_2^2 - \|\epsilon^l - \epsilon_{\text{ref}}(x_t^l, t)\|_2^2))), \quad (1)$$

where $x_t^* = \alpha_t x_0^* + \sigma_t \epsilon^*$, $\epsilon^* \sim \mathcal{N}(0, I)$. And $\lambda_t = \frac{\alpha_t^2}{\sigma_t^2}$ is the signal-to-noise ratio. However, this uniform weighting strategy in Diffusion-DPO proves suboptimal for the nuanced demands of multi-subject generation. By treating all spatial regions with equal importance, the approach is inherently susceptible to interference from irrelevant background details. Consequently, its efficacy in preserving the consistency and identity of multiple subjects within a single composition is significantly constrained. To overcome this limitation, a more targeted weighting mechanism is necessary—one that can distinguish between foreground subjects and the background, focusing optimization where most needed.

4 Method

We propose **Disrupted-Instance Pair Dataset (DIP)** and **Focus Direct Preference Optimization (FocusDPO)**, a spatially-aware preference optimization framework for addressing subject-level inconsistencies in personalized image generation. Our method constructs high-quality subject-consistent pairs $\{(x_0^w, x_0^l)\}$ with controlled subject variation, utilizing a binary prior guidance $\mathbf{M}_{\text{prior}} \in \{0, 1\}^{H \times W}$ to identify regions containing subject differences. We then introduce a spatial weighting mechanism $\mathbf{M} \in \mathbb{R}^{H \times W}$ that dynamically modulates the optimization process across different regions, where H and W denote the height and width of the latent feature maps.

4.1 Disrupted-Instance Pair Dataset

We construct the DIP Dataset as a semantically aligned collection of positive-negative image pairs designed to isolate subject-level inconsistencies. Each image pair maintains semantic content parity while introducing

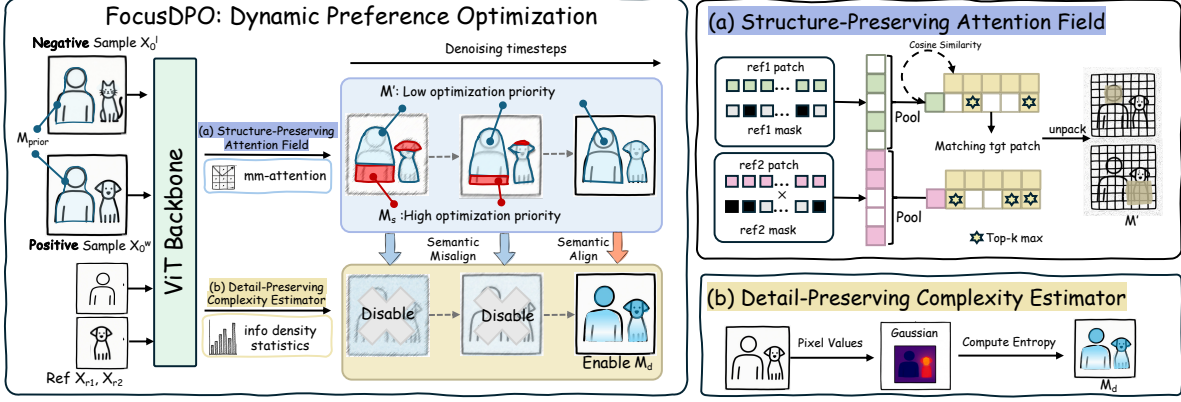


Figure 4 The overall framework of FocusDPO. FocusDPO introduce a *spatially-aware optimization framework* (left) that adaptively focuses on critical regions through dynamic semantic guidance, leveraging (a) *Structure-Preserving Attention Field* and (b) *Detail-Preserving Complexity Estimator*.

localized perturbations to subject regions. We begin by synthesizing reference and target pairs $\{(x_r, x_0^w)\}$ using the FLUX generator [17], conditioned on identical subject prompts c but with varied auxiliary attributes such as background and lighting. From the resulting corpus, we manually curate 5,000 high-quality pairs for single-subject and multi-subject scenario, where x_0^w shows strong visual alignment with x_r in subject identity, serving as **positive samples**.

To construct **negative samples** x_0^l , we introduce controlled semantic disruptions to x_0^w while preserving surrounding context. We apply GroundingSAM2 [20, 30] to extract accurate binary segmentation maps M_{prior} that isolate subject regions. To maintain semantic consistency in the altered regions, we utilize GPT-4o to generate fine-grained captions for the segmented areas, providing detailed semantic descriptions. These captions are fed into the inpainting model [17], which modifies subject-relevant pixels while preserving surrounding context. The resulting image x_0^l exhibits degraded visual consistency with respect to x_r while maintaining overall semantic coherence.

The final DIP dataset comprises quadruplets (c, x_r, x_0^w, x_0^l) , with shared conditioning prompt c and reference image x_r specifying target subject identity, a high-consistency image x_0^w maintaining strong alignment with reference x_r , and a low-consistency counterpart x_0^l generated through localized semantic perturbation within M_{prior} . This approach ensures subject-level consistency in preference learning while removing confounders, forming the basis for spatially-aware optimization in FocusDPO.

4.2 Focus Direct Preference Optimization

To overcome the limitations of uniform weighting in existing methods, we introduce a spatially-aware optimization framework, as shown in Fig. 4. The cornerstone of our approach is a dynamic semantic guidance strategy that adaptively focuses supervisory signals on critical regions by decomposing the task into two complementary sub-problems: preserving global consistency via a Structure-Preserving Attention Field and maintaining high-fidelity features with a Detail-Preserving Complexity Estimator. We leverage these components to inform a spatial weighting mechanism that dynamically modulates the optimization process across semantically critical and non-critical regions.

Structure-Preserving Attention Field: Contemporary personalized generation methods suffer from subject confusion, where target attributes propagate to semantically unrelated regions, especially in multi-subject generation scenarios. Our primary objective is to address these structural deficiencies in generated images. Multi-modal attention layers inherently encode semantic relationships between the noised latent representation x_t and the reference image x_r . For each attention layer i , we denote the target and reference token embeddings

as:

$$\begin{cases} H_{x_t}^i \in \mathbb{R}^{p_{x_t} \times d}, \\ H_{x_r}^i \in \mathbb{R}^{p_{x_r} \times d}, \end{cases} \quad i \in \{0, 1, \dots, N-1\}, \quad (2)$$

where p_{x_t} and p_{x_r} denote the number of patch tokens, d is the embedding dimension, and N is the total number of multi-modal attention layers.

To establish semantic correspondences between subject regions and target patches, we employ a cross-layer correspondence strategy. For each reference subject patch j , we identify the target location with maximal semantic alignment by computing:

$$\begin{aligned} S &= \sum_{i=1}^N \frac{1}{N} \cdot \left\langle \frac{CLS_{x_r}^i}{|CLS_{x_r}^i|^2}, \frac{H_{x_t}^i}{|H_{x_t}^i|^2} \right\rangle, \\ CLS_{x_r}^i &= \text{pool}(H_{x_r}^i), \quad CLS_{x_r}^i \in \mathbb{R}^{1 \times d}. \end{aligned} \quad (3)$$

Let S be the score vector of size $1 \times p_{x_t}$, with elements S_i for $i = 1, \dots, p_{x_t}$. We identify the set of indices \mathcal{J} corresponding to the K largest scores in S :

$$\mathcal{J} = \arg \max_{i=1, \dots, p_{x_t}} (S_i), \quad (4)$$

where K is the number of tokens of reference image x_r in x_t . Using this set, we construct a binary attention map M' where element M'_j is set to 1 if its index j is in the set of top- K indices \mathcal{J} , and 0 otherwise:

$$M'_j = \mathbb{I}(j \in \mathcal{J}). \quad (5)$$

Finally, we define Structure-Preserving Attention Field as:

$$M_s = M_{\text{prior}} \setminus M'. \quad (6)$$

Detail-Preserving Complexity Estimator: Conventional preference optimization methods treat preference distinctions as globally distributed properties. However, for multi-subject generation in complex scenes, preference signals are often spatially localized. We observe that preference-critical regions correlate with areas of high visual complexity, which also pose challenges for diffusion model reconstruction. Motivated by this observation, we introduce a Detail-Preserving Complexity Estimator that prioritizes these complex regions during preference optimization through an information density weighting mechanism.

Our method generates this weight mask through two core steps. First, we compute a visual complexity score for each local region. For a patch centered at pixel p , denoted as patch_p , we obtain its complexity score C_p by calculating the Shannon entropy of its grayscale pixel intensity distribution [15]. Higher entropy values signify richer textures and details corresponding to higher visual complexity, while smooth and uniform regions yield lower entropy:

$$C_p = \text{CalculateComplexity}(\text{patch}_p). \quad (7)$$

Second, to ensure these scores are comparable and form a usable weighting scheme, we perform global normalization. We scale the complexity score C_p of each location to the range $[0, 1]$ to obtain the final information complexity M_d :

$$M_d = \frac{C_p - C_{\min}}{C_{\max} - C_{\min}}, \quad (8)$$

where C_{\min} and C_{\max} represent the minimum and maximum complexity scores computed across all local regions of the entire image. The resulting matrix of weights M_d constitutes our Detail-Preserving Complexity Estimator.

By incorporating this complexity estimator into the model’s optimization loss function, we guide the model to focus attention on regions with higher weights during training. This enables the model to preferentially learn from and correct errors in critical areas such as fine textures and facial details, thereby significantly enhancing the local quality and overall fidelity of generated images.

Algorithm 1 FocusDPO Training Algorithm

```
1: procedure COMPUTEMASKS( $x_0^w, x_t^w, x_r$ )
2:   Compute the Structure-Preserving Attention Field  $\mathbf{M}_s$  based on Eq. 3-Eq. 6.
3:   Compute the Detail-Preserving Complexity Estimator  $\mathbf{M}_d$  based on Eq. 7 and Eq. 8.
4:   return  $\mathbf{M}_s, \mathbf{M}_d$ 
5: end procedure

6: for each training step do
7:   Sample preference pair  $(x_0^w, x_0^l, \mathbf{M}_{\text{prior}}) \sim \mathcal{D}$ , timestep  $t \sim \mathcal{U}(1, T)$ , noise  $\epsilon \sim \mathcal{N}(0, I)$ .
8:   Create noised latents  $x_t^w, x_t^l$ .

   Step 1: Generate dynamic semantic masks
9:    $\mathbf{M}_s, \mathbf{M}_d \leftarrow \text{COMPUTEMASKS}(x_0^w, x_t^w, x_r)$ 

   Step 2: Calculate the focus coverage ratio
10:   $A_{\text{focus}} \leftarrow \|\mathbf{M}_s\|_1 / \|\mathbf{M}_{\text{prior}}\|_1$ 

   Step 3: Determine fusion mask  $\mathbf{M}$ 
11:  Determine fusion mask  $\mathbf{M}$  using Eq. 9.

   Step 4: Compute loss and update model
12:  Compute the final loss  $\mathcal{L}_{\text{FocusDPO}}$  using the spatially weighted objective (Eq. 10).
13:  Update model parameters:  $\theta \leftarrow \theta - \eta \nabla_{\theta} \mathcal{L}_{\text{FocusDPO}}$ .
14: end for
```

Final Loss: As shown in Alg. 1, we determine the dynamic fusion field \mathbf{M} through an adaptive strategy that leverages both structural and detail-preserving components. The fusion mechanism employs a focus threshold $\tau = 0.1$ and tradeoff parameter $\gamma = 0.3$ to balance global consistency and local fidelity (*with ablation study in appendix*):

$$\mathbf{M} = \begin{cases} \mathbf{M}_s, & A_{\text{focus}} > \tau \\ \gamma \mathbf{M}_s + (1 - \gamma) \mathbf{M}_d \odot \mathbf{M}_{\text{prior}}, & A_{\text{focus}} \leq \tau \end{cases} \quad (9)$$

The complete FocusDPO objective incorporates the spatial fusion field into the preference optimization framework:

$$\begin{aligned} \mathcal{L}_{\text{FocusDPO}}(\theta) = & -\mathbb{E} \log \sigma(-\beta T \omega(\lambda_t) (\|(\epsilon^w - \epsilon_{\theta}(x_t^w, t)) \odot \mathbf{M}\|_2^2 - \|(\epsilon^w - \epsilon_{\text{ref}}(x_t^w, t)) \odot \mathbf{M}\|_2^2 \\ & - (\|(\epsilon^l - \epsilon_{\theta}(x_t^l, t)) \odot \mathbf{M}\|_2^2 - \|(\epsilon^l - \epsilon_{\text{ref}}(x_t^l, t)) \odot \mathbf{M}\|_2^2)). \end{aligned} \quad (10)$$

This spatially-aware framework enables the model to preferentially learn from and correct errors in critical regions, significantly enhancing local quality and overall fidelity of generated images while maintaining subject consistency across complex multi-subject scenarios.

5 Experiments

5.0.1 Implementation Details

We implement our FocusDPO methodology on two representative diffusion architectures: U-Net [31] and DiT [25], ensuring broad applicability and generalizability. For SDXL, we use the pre-trained IP-Adapter-Plus [40] with the SDXL [26] text-to-image model, consistent with PatchDPO [13]. For DiT, we integrate FocusDPO into the UNO [37] pipeline for multi-subject synthesis, utilizing FLUX.1 dev [17] as the foundation model.

Our training uses rank-32 LoRA [10] modules in both backbones, trained for 2000 steps on 8 GPUs with AdamW (lr=1e-8, batch size=1 per GPU). The training dataset DIP contains 10,000 preference pairs (5000 each for

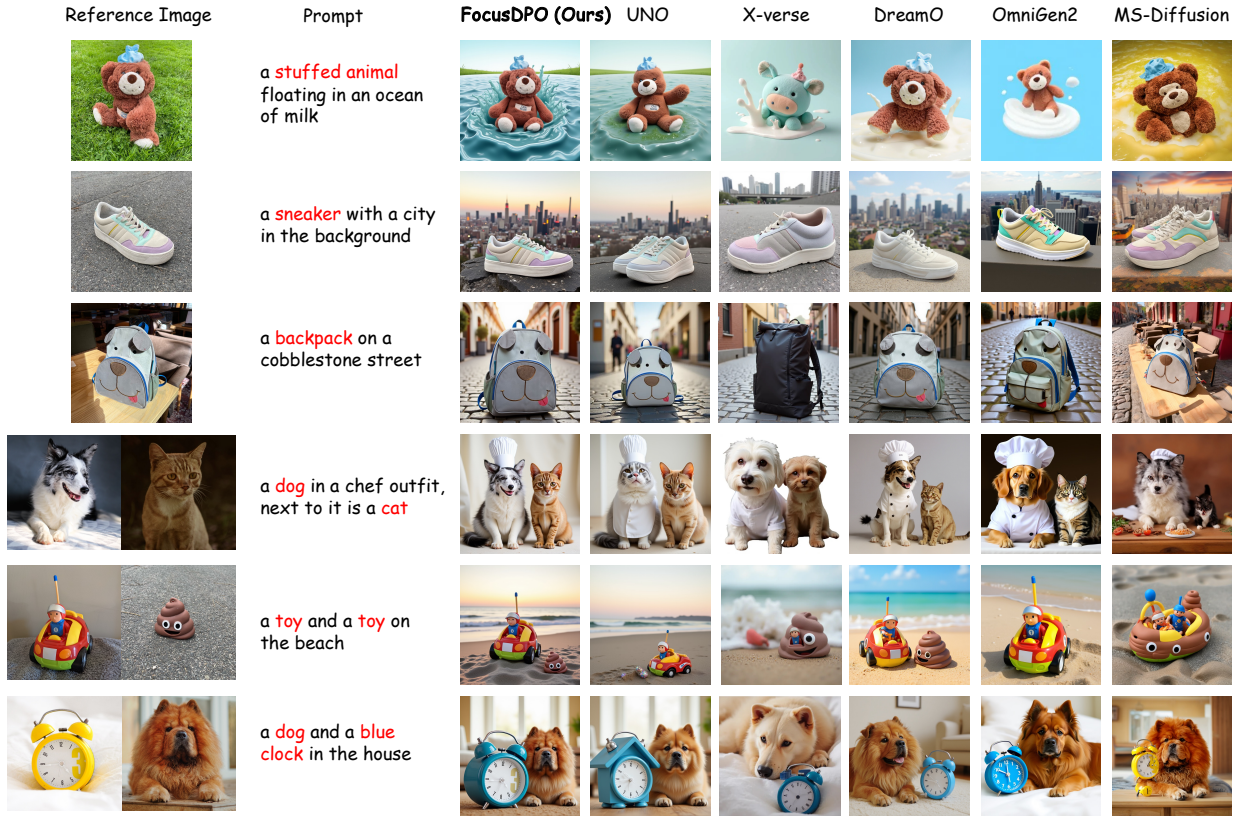


Figure 5 Qualitative comparison of single-subject and multi-subject generation with different methods on DreamBench.

single- and multi-subject generation). The test dataset is DreamBench [32], which includes both single-subject and multi-subject cases, with the multi-subject evaluation protocol following settings in [14, 21, 37].

5.0.2 Evaluation Metrics

We evaluate subject fidelity and text-image alignment using established metrics. Subject fidelity is measured through CLIP-I [28] and DINO [24] scores, computing cosine similarity between generated, and reference images and text-image alignment is assessed using CLIP-T score.

5.1 Qualitative Analysis

We conduct a comprehensive comparative evaluation of our proposed methodology against existing state-of-the-art approaches across both single-subject and multi-subject generation paradigms. Our comparative analysis encompasses five recent and competitive methods: Xverse [4], DreamO [23], OmniGen2 [36], MS-Diffusion [35], and our backbone architecture UNO [37]. As demonstrated in Fig. 5, FocusDPO exhibits superior performance in maintaining subject consistency and identity preservation while simultaneously ensuring global semantic coherence. The performance gains arise from our training paradigm, which dynamically targets complex, detail-rich regions to better capture subject-specific features and preserve fine-grained identity—especially in multi-subject generation.

5.2 Quantitative comparisons

Tables 1 and 2 present comprehensive quantitative evaluations of our method against competing approaches on the DreamBench dataset for single-object and multi-subject personalized generation, respectively. We

Method	DINO ↑	CLIP-I ↑	CLIP-T ↑
DreamBooth [32]	0.668	0.803	0.305
SSR-Encoder [42]	0.612	0.821	0.308
RealCustom++ [22]	0.702	0.794	0.318
OmniGen [38]	0.693	0.801	0.315
OminiControl [33]	0.684	0.799	0.312
DreamO [23]	0.712	0.809	0.314
IP-Adapter-Plus [40]	0.692	0.826	0.281
IP-Adapter-Plus + SFT	0.691	0.828	0.279
IP-Adapter-Plus + DPO	0.695	0.831	0.276
IP-Adapter-Plus + PatchDPO	0.727	0.838	0.292
IP-Adapter-Plus + FocusDPO	0.751	<u>0.840</u>	0.303
UNO [37]	0.760	0.835	0.304
UNO + SFT	0.761	0.832	0.299
UNO + DPO	<u>0.764</u>	0.835	0.301
UNO + FocusDPO	0.802	0.842	<u>0.316</u>

Table 1 Performance comparison for single-object personalized generation on DreamBench [32]. The best result is marked in **bold**, and the second-best is underlined.

Method	DINO ↑	CLIP-I ↑	CLIP-T ↑
DreamBooth [32]	0.430	0.695	0.308
MIP-Adapter [14]	0.482	0.726	0.311
MS-Diffusion [35]	0.525	0.726	0.319
OmniGen [38]	0.511	0.722	0.331
DreamO [23]	0.539	0.727	0.313
UNO (DiT Backbone)	0.542	<u>0.733</u>	0.322
UNO + SFT	0.542	0.732	0.321
UNO + DPO	<u>0.545</u>	0.731	0.322
UNO + FocusDPO	0.570	0.739	<u>0.328</u>

Table 2 Multi-subject synthesis results on DreamBench.

conduct evaluations of FocusDPO across two distinct backbone architectures, demonstrating consistent performance gains across all metrics. When integrated with the UNO backbone, FocusDPO establishes new state-of-the-art results, achieving a 5.5% improvement on DINO (0.802 vs. 0.760) for single-object generation, and state-of-the-art performance (DINO: 0.570, CLIP-I: 0.739) for multi-subject synthesis. These empirical results substantiate the efficacy of our proposed framework.

5.3 Ablation Study

5.3.1 Ablation on Dynamic Fusion Components

In Fig. 6, We conduct an ablation study to analyze the contribution of two critical weighting components within our dynamic optimization framework: the Structure-Preserving Attention Field \mathbf{M}_s and the Detail-Preserving Complexity Estimator \mathbf{M}_d . The supplementary experimental results presented in Fig. 7 demonstrate that the absence of \mathbf{M}_s results in substantial subject disambiguation failures, with this degradation being particularly pronounced in multi-subject synthesis scenarios. Conversely, the omission of \mathbf{M}_d manifests as inconsistencies in fine-grained structural coherence across the generated outputs. These results confirm that \mathbf{M}_s and \mathbf{M}_d work in tandem to preserve semantic alignment and enhance structural fidelity in complex regions.

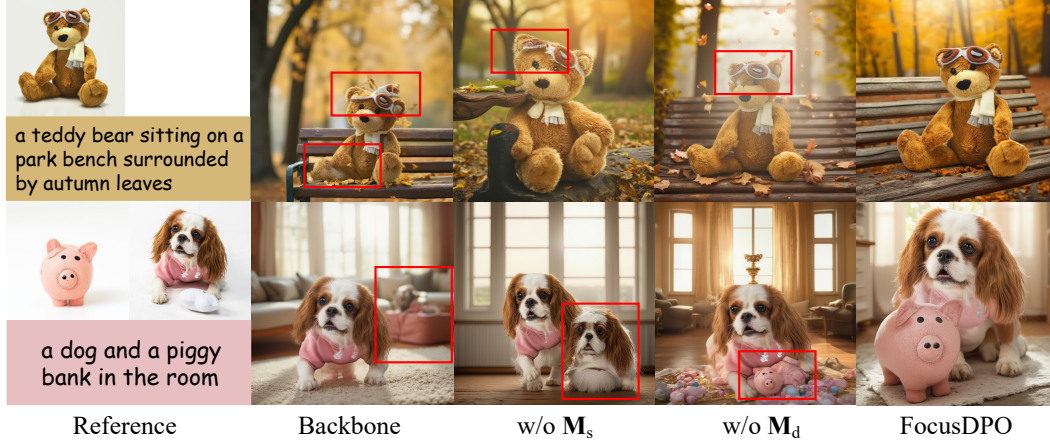


Figure 6 Ablation study on dynamic weighting components.

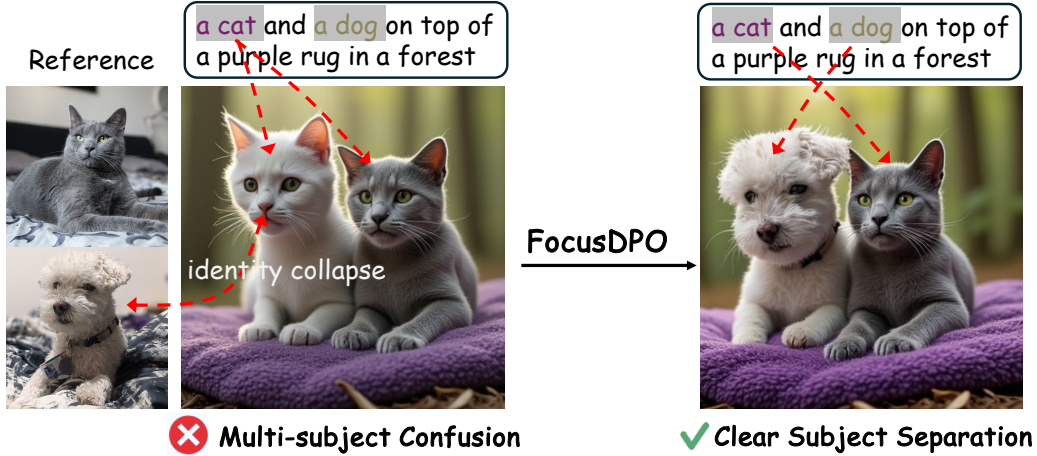


Figure 7 Analysis of resolving semantic confusion.

5.3.2 Ablation on Optimization Strategy

We evaluate our dynamic optimization approach by comparing three training paradigms across two backbone architectures using the generated DIP dataset: supervised fine-tuning (SFT), standard DPO, and our FocusDPO methodology. As shown in Tab. 1, FocusDPO consistently outperforms both SFT and conventional DPO across all metrics. For single-subject scenarios, FocusDPO achieves 0.751 under IPAP (8.7% improvement over SFT, 8.1% over DPO) and 0.802 under UNO (5.4% improvement over SFT, 5.0% over DPO). For multi-subject scenarios under UNO, FocusDPO achieves 0.570 (DINO), 0.739 (CLIP-I), and 0.326 (CLIP-T), representing improvements of 5.2%/4.6% (DINO), 1.0%/1.1% (CLIP-I), and 1.6%/1.2% (CLIP-T) over SFT/DPO respectively. These results demonstrate that improvements stem from our optimization strategy rather than dataset biases.

6 Conclusion

We present FocusDPO, a framework for multi-subject personalized image generation that tackles the challenge of preserving subject identity while avoiding attribute confusion. Our method introduces dynamic focus modulation mechanism that dynamically prioritize regions based on supervision complexity and semantic alignment. Extensive experiments show that FocusDPO consistently improves pre-trained models, achieving state-of-the-art results on both single- and multi-subject benchmarks, setting a new standard for controllable multi-subject generation.

References

- [1] Yuntao Bai, Andy Jones, Kamal Ndousse, Amanda Askell, Anna Chen, Nova DasSarma, Dawn Drain, Stanislav Fort, Deep Ganguli, Tom Henighan, et al. Training a helpful and harmless assistant with reinforcement learning from human feedback. arXiv preprint arXiv:2204.05862, 2022.
- [2] Kevin Black, Michael Janner, Yilun Du, Ilya Kostrikov, and Sergey Levine. Training diffusion models with reinforcement learning. arXiv preprint arXiv:2305.13301, 2023.
- [3] Stephen Casper, Xander Davies, Claudia Shi, Thomas Krendl Gilbert, Jérémy Scheurer, Javier Rando, Rachel Freedman, Tomasz Korbak, David Lindner, Pedro Freire, et al. Open problems and fundamental limitations of reinforcement learning from human feedback. arXiv preprint arXiv:2307.15217, 2023.
- [4] Bowen Chen, Mengyi Zhao, Haomiao Sun, Li Chen, Xu Wang, Kang Du, and Xinglong Wu. Xverse: Consistent multi-subject control of identity and semantic attributes via dit modulation. arXiv preprint arXiv:2506.21416, 2025.
- [5] Nan Chen, Mengqi Huang, Zhuowei Chen, Yang Zheng, Lei Zhang, and Zhendong Mao. Customcontrast: A multilevel contrastive perspective for subject-driven text-to-image customization, 2025.
- [6] Kevin Clark, Paul Vicol, Kevin Swersky, and David J Fleet. Directly fine-tuning diffusion models on differentiable rewards. arXiv preprint arXiv:2309.17400, 2023.
- [7] Ying Fan, Olivia Watkins, Yuqing Du, Hao Liu, Moonkyung Ryu, Craig Boutilier, Pieter Abbeel, Mohammad Ghavamzadeh, Kangwook Lee, and Kimin Lee. Dpok: Reinforcement learning for fine-tuning text-to-image diffusion models. Advances in Neural Information Processing Systems, 36:79858–79885, 2023.
- [8] Rinon Gal, Yuval Alaluf, Yuval Atzmon, Or Patashnik, Amit H Bermano, Gal Chechik, and Daniel Cohen-Or. An image is worth one word: Personalizing text-to-image generation using textual inversion. arXiv preprint arXiv:2208.01618, 2022.
- [9] Jonathan Ho, Ajay Jain, and Pieter Abbeel. Denoising diffusion probabilistic models. Advances in neural information processing systems, 33:6840–6851, 2020.
- [10] Edward J. Hu, Yelong Shen, Phillip Wallis, Zeyuan Allen-Zhu, Yanzhi Li, Shean Wang, Lu Wang, and Weizhu Chen. Lora: Low-rank adaptation of large language models. In The Tenth International Conference on Learning Representations, ICLR 2022, Virtual Event, April 25-29, 2022.
- [11] Lianghua Huang, Wei Wang, Zhi-Fan Wu, Yupeng Shi, Huanzhang Dou, Chen Liang, Yutong Feng, Yu Liu, and Jingren Zhou. In-context lora for diffusion transformers. CoRR, abs/2410.23775, 2024.
- [12] Mengqi Huang, Zhendong Mao, Mingcong Liu, Qian He, and Yongdong Zhang. Realcustom: Narrowing real text word for real-time open-domain text-to-image customization. CoRR, abs/2403.00483, 2024.
- [13] Qihan Huang, Long Chan, Jinlong Liu, Wanggui He, Hao Jiang, Mingli Song, and Jie Song. Patchdpo: Patch-level DPO for finetuning-free personalized image generation. In IEEE/CVF Conference on Computer Vision and Pattern Recognition, CVPR 2025, Nashville, TN, USA, June 11-15, 2025, pages 18369–18378. Computer Vision Foundation / IEEE, 2025.
- [14] Qihan Huang, Siming Fu, Jinlong Liu, Hao Jiang, Yipeng Yu, and Jie Song. Resolving multi-condition confusion for finetuning-free personalized image generation. In AAAI-25, Sponsored by the Association for the Advancement of Artificial Intelligence, February 25 - March 4, 2025, Philadelphia, PA, USA, pages 3707–3714, 2025.
- [15] Weinan Jia, Mengqi Huang, Nan Chen, Lei Zhang, and Zhendong Mao. D²it: Dynamic diffusion transformer for accurate image generation. In Proceedings of the IEEE/CVF Conference on Computer Vision and Pattern Recognition (CVPR), pages 12860–12870, June 2025.
- [16] Nupur Kumari, Bingliang Zhang, Richard Zhang, Eli Shechtman, and Jun-Yan Zhu. Multi-concept customization of text-to-image diffusion. In Proceedings of the IEEE/CVF conference on computer vision and pattern recognition, pages 1931–1941, 2023.
- [17] Black Forest Labs. Flux. <https://github.com/black-forest-labs/flux>, 2024.
- [18] Kimin Lee, Hao Liu, Moonkyung Ryu, Olivia Watkins, Yuqing Du, Craig Boutilier, Pieter Abbeel, Mohammad Ghavamzadeh, and Shixiang Shane Gu. Aligning text-to-image models using human feedback. arXiv preprint arXiv:2302.12192, 2023.

- [19] Dongxu Li, Junnan Li, and Steven C. H. Hoi. Blip-diffusion: Pre-trained subject representation for controllable text-to-image generation and editing. In Advances in Neural Information Processing Systems 36: Annual Conference on Neural Information Processing Systems 2023, NeurIPS 2023, New Orleans, LA, USA, December 10 - 16, 2023, 2023.
- [20] Shilong Liu, Zhaoyang Zeng, Tianhe Ren, Feng Li, Hao Zhang, Jie Yang, Chunyuan Li, Jianwei Yang, Hang Su, Jun Zhu, et al. Grounding dino: Marrying dino with grounded pre-training for open-set object detection. arXiv preprint arXiv:2303.05499, 2023.
- [21] Jian Ma, Junhao Liang, Chen Chen, and Haonan Lu. Subject-diffusion: Open domain personalized text-to-image generation without test-time fine-tuning. In ACM SIGGRAPH 2024 Conference Papers, SIGGRAPH 2024, Denver, CO, USA, 27 July 2024- 1 August 2024, page 25. ACM, 2024.
- [22] Zhendong Mao, Mengqi Huang, Fei Ding, Mingcong Liu, Qian He, and Yongdong Zhang. Realcustom++: Representing images as real-word for real-time customization. arXiv preprint arXiv:2408.09744, 2024.
- [23] Chong Mou, Yanze Wu, Wenxu Wu, Zinan Guo, Pengze Zhang, Yufeng Cheng, Yiming Luo, Fei Ding, Shiwen Zhang, Xinghui Li, Mengtian Li, Songtao Zhao, Jian Zhang, Qian He, and Xinglong Wu. Dreamo: A unified framework for image customization. CoRR, abs/2504.16915, 2025.
- [24] Maxime Oquab, Timothée Darcet, Théo Moutakanni, Huy V. Vo, Marc Szafraniec, Vasil Khalidov, Pierre Fernandez, Daniel Haziza, Francisco Massa, Alaaeldin El-Nouby, Mido Assran, Nicolas Ballas, Wojciech Galuba, Russell Howes, Po-Yao Huang, Shang-Wen Li, Ishan Misra, Michael Rabbat, Vasu Sharma, Gabriel Synnaeve, Hu Xu, Hervé Jégou, Julien Mairal, Patrick Labatut, Armand Joulin, and Piotr Bojanowski. Dinov2: Learning robust visual features without supervision. Trans. Mach. Learn. Res., 2024, 2024.
- [25] William Peebles and Saining Xie. Scalable diffusion models with transformers. In Proceedings of the IEEE/CVF international conference on computer vision, pages 4195–4205, 2023.
- [26] Dustin Podell, Zion English, Kyle Lacey, Andreas Blattmann, Tim Dockhorn, Jonas Müller, Joe Penna, and Robin Rombach. SDXL: improving latent diffusion models for high-resolution image synthesis. In The Twelfth International Conference on Learning Representations, ICLR 2024, Vienna, Austria, May 7-11, 2024, 2024.
- [27] Mihir Prabhudesai, Anirudh Goyal, Deepak Pathak, and Katerina Fragkiadaki. Aligning text-to-image diffusion models with reward backpropagation. 2023.
- [28] Alec Radford, Jong Wook Kim, Chris Hallacy, Aditya Ramesh, Gabriel Goh, Sandhini Agarwal, Girish Sastry, Amanda Askell, Pamela Mishkin, Jack Clark, Gretchen Krueger, and Ilya Sutskever. Learning transferable visual models from natural language supervision. In Proceedings of the 38th International Conference on Machine Learning, ICML 2021, 18-24 July 2021, Virtual Event, volume 139, pages 8748–8763. PMLR, 2021.
- [29] Rafael Rafailov, Archit Sharma, Eric Mitchell, Christopher D Manning, Stefano Ermon, and Chelsea Finn. Direct preference optimization: Your language model is secretly a reward model. Advances in neural information processing systems, 36:53728–53741, 2023.
- [30] Nikhila Ravi, Valentin Gabeur, Yuan-Ting Hu, Ronghang Hu, Chaitanya Ryali, Tengyu Ma, Haitham Khedr, Roman Rädle, Chloe Rolland, Laura Gustafson, Eric Mintun, Junting Pan, Kalyan Vasudev Alwala, Nicolas Carion, Chao-Yuan Wu, Ross Girshick, Piotr Dollár, and Christoph Feichtenhofer. Sam 2: Segment anything in images and videos, 2024. URL <https://arxiv.org/abs/2408.00714>.
- [31] Robin Rombach, Andreas Blattmann, Dominik Lorenz, Patrick Esser, and Björn Ommer. High-resolution image synthesis with latent diffusion models. In Proceedings of the IEEE/CVF conference on computer vision and pattern recognition, pages 10684–10695, 2022.
- [32] Nataniel Ruiz, Yuanzhen Li, Varun Jampani, Yael Pritch, Michael Rubinstein, and Kfir Aberman. Dreambooth: Fine tuning text-to-image diffusion models for subject-driven generation. In Proceedings of the IEEE/CVF conference on computer vision and pattern recognition, pages 22500–22510, 2023.
- [33] Zhenxiong Tan, Songhua Liu, Xingyi Yang, Qiaochu Xue, and Xinchao Wang. Ominicontrol: Minimal and universal control for diffusion transformer. CoRR, abs/2411.15098, 2024.
- [34] Bram Wallace, Meihua Dang, Rafael Rafailov, Linqi Zhou, Aaron Lou, Senthil Purushwalkam, Stefano Ermon, Caiming Xiong, Shafiq Joty, and Nikhil Naik. Diffusion model alignment using direct preference optimization. In IEEE/CVF Conference on Computer Vision and Pattern Recognition, CVPR 2024, Seattle, WA, USA, June 16-22, 2024, pages 8228–8238, 2024.

- [35] Xierui Wang, Siming Fu, Qihan Huang, Wanggui He, and Hao Jiang. Ms-diffusion: Multi-subject zero-shot image personalization with layout guidance. In The Thirteenth International Conference on Learning Representations, ICLR 2025, Singapore, April 24-28, 2025, 2025.
- [36] Chenyuan Wu, Pengfei Zheng, Ruiran Yan, Shitao Xiao, Xin Luo, Yueze Wang, Wanli Li, Xiyan Jiang, Yexin Liu, Junjie Zhou, Ze Liu, Ziyi Xia, Chaofan Li, Haoge Deng, Jiahao Wang, Kun Luo, Bo Zhang, Defu Lian, Xinlong Wang, Zhongyuan Wang, Tiejun Huang, and Zheng Liu. Omnigen2: Exploration to advanced multimodal generation. CoRR, abs/2506.18871, 2025.
- [37] Shaojin Wu, Mengqi Huang, Wenxu Wu, Yufeng Cheng, Fei Ding, and Qian He. Less-to-more generalization: Unlocking more controllability by in-context generation. arXiv preprint arXiv:2504.02160, 2025.
- [38] Shitao Xiao, Yueze Wang, Junjie Zhou, Huaying Yuan, Xingrun Xing, Ruiran Yan, Chaofan Li, Shuting Wang, Tiejun Huang, and Zheng Liu. Omnigen: Unified image generation. In IEEE/CVF Conference on Computer Vision and Pattern Recognition, CVPR 2025, Nashville, TN, USA, June 11-15, 2025, pages 13294–13304. Computer Vision Foundation / IEEE, 2025.
- [39] Yiming Xie, Varun Jampani, Lei Zhong, Deqing Sun, and Huaizu Jiang. Omnicontrol: Control any joint at any time for human motion generation. arXiv preprint arXiv:2310.08580, 2023.
- [40] Hu Ye, Jun Zhang, Sibio Liu, Xiao Han, and Wei Yang. Ip-adapter: Text compatible image prompt adapter for text-to-image diffusion models. CoRR, abs/2308.06721, 2023.
- [41] Yongcheng Zeng, Guoqing Liu, Weiyu Ma, Ning Yang, Haifeng Zhang, and Jun Wang. Token-level direct preference optimization. arXiv preprint arXiv:2404.11999, 2024.
- [42] Yuxuan Zhang, Yiren Song, Jiaming Liu, Rui Wang, Jinpeng Yu, Hao Tang, Huaxia Li, Xu Tang, Yao Hu, Han Pan, and Zhongliang Jing. Ssr-encoder: Encoding selective subject representation for subject-driven generation. In IEEE/CVF Conference on Computer Vision and Pattern Recognition, CVPR 2024, Seattle, WA, USA, June 16-22, 2024, pages 8069–8078. IEEE, 2024.
- [43] Zhanhui Zhou, Jie Liu, Chao Yang, Jing Shao, Yu Liu, Xiangyu Yue, Wanli Ouyang, and Yu Qiao. Beyond one-preference-for-all: Multi-objective direct preference optimization. 2023.

Appendix

A Supplementary Ablation Study

A.1 Optimization Strategy Performance Analysis

To evaluate the effectiveness of our FocusDPO, we conduct ablation studies across two architectural backbones: U-Net and Diffusion Transformer (DiT). For the U-Net architecture, we employ SDXL [26] with IP-Adapter [40] as our baseline implementation.

Comparative Evaluation Framework. Our ablation study isolates the contributions of the proposed optimization strategy from potential confounding factors including dataset artifacts and inherent DPO characteristics. The quantitative results presented in Section 4.3 are complemented by qualitative comparisons illustrated in Fig. 8, providing a comprehensive assessment across multiple evaluation dimensions. As shown in Fig. 8, FocusDPO exhibits superior identity consistency preservation compared to existing optimization paradigms. The qualitative results reveal marked improvements across two critical dimensions:

- **Semantic Fidelity:** Enhanced preservation of subject-specific characteristics and attributes
- **Visual Consistency:** Improved coherence in appearance and structural details across generated samples

Comparison with Prior Work. FocusDPO maintains robust identity preservation even when deployed on constrained architectures such as SDXL+IP-Adapter, indicating the generalizability of our optimization approach. Notably, FocusDPO substantially outperforms PatchDPO [13]—the sole prior work applying DPO principles to consistency-aware generation tasks. This performance advantage stems from our novel integration of:

- Dynamic semantic attention mechanisms that adapt to content complexity
- Adaptive detail preservation strategies that maintain fine-grained visual fidelity

These findings validate both the theoretical foundations and practical efficacy of our approach across diverse architectural configurations.

A.2 Analysis on $\mathbf{M}_{\text{prior}}$

Building upon the ablation studies presented in Section 4.3, which examined the individual contributions of \mathbf{M}_s and \mathbf{M}_d , we extend our analysis to investigate the influence of the prior mask $\mathbf{M}_{\text{prior}}$ on the overall framework performance. Our investigation reveals that $\mathbf{M}_{\text{prior}}$ exhibits a dual functionality: it serves as a superset constraint for Structure-Preserving Attention Field \mathbf{M}_s while simultaneously constraining the Detail-Preserving Complexity Estimator \mathbf{M}_d . To systematically isolate and quantify the impact of $\mathbf{M}_{\text{prior}}$, we design three targeted ablation configurations.

Configuration I: Prior-only baseline. (*w/o* \mathbf{M}_s & \mathbf{M}_d) This configuration eliminates both semantic alignment and detail preservation components, focusing exclusively on the prior mask influence. The masking strategy reduces to $\mathbf{M} = \mathbf{M}_{\text{prior}}$, effectively providing a baseline for understanding the fundamental contribution of spatial priors.

Configuration II: Information complexity Only. (*w/o* \mathbf{M}_s & $\mathbf{M}_{\text{prior}}$) This variant removes both the semantic structure alignment mask \mathbf{M}_s and the spatial constraints imposed by $\mathbf{M}_{\text{prior}}$ on the information density mask, resulting in $\mathbf{M} = \mathbf{M}_d$. This configuration evaluates the effectiveness of information density guidance in isolation.

Configuration III: Region Unconstrained information complexity. (*w/o* $\mathbf{M}_{\text{prior}}$) This configuration retains the semantic mask \mathbf{M}_s while removing the spatial constraints of $\mathbf{M}_{\text{prior}}$ on \mathbf{M}_d . The dynamic fusion strategy becomes:

$$\mathbf{M} = \begin{cases} \mathbf{M}_s, & A_{\text{focus}} > \tau \\ \gamma \mathbf{M}_s + (1 - \gamma) \mathbf{M}_d, & A_{\text{focus}} \leq \tau \end{cases} \quad (11)$$



Figure 8 Qualitative comparison of identity preservation across different optimization methods.

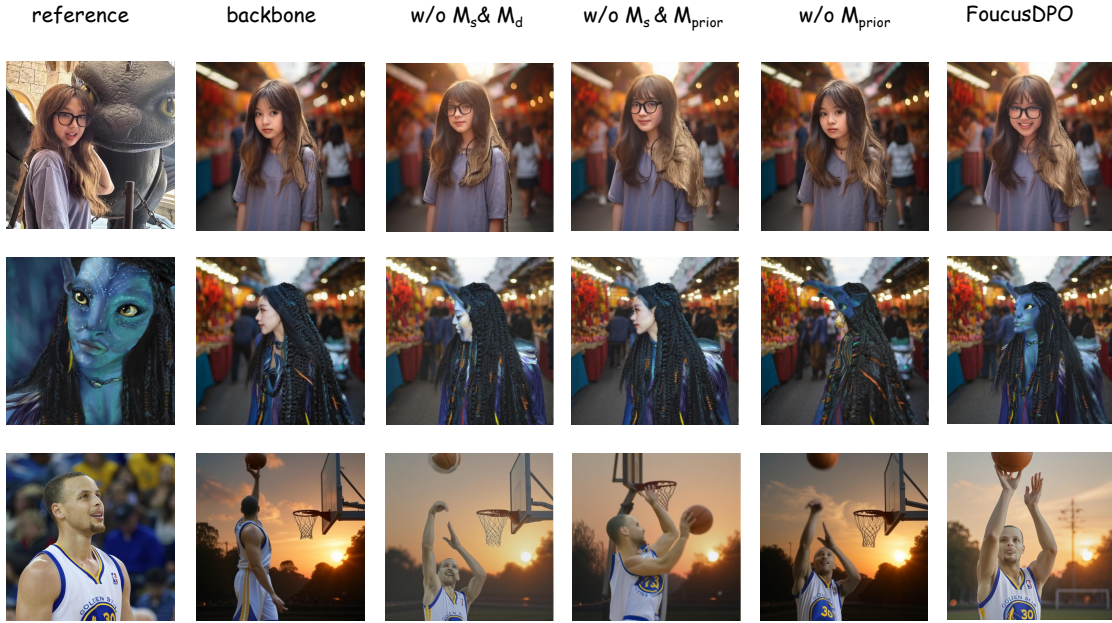


Figure 9 Ablation study on the prior mask M_{prior} component. The proposed FocusDPO outperforms all ablation variants, demonstrating the effectiveness of the integrated dynamic fusion optimization strategy.

The comparative results presented in Fig. 9 demonstrate that while each ablation configuration yields marginal improvements in consistency metrics, their performance remains substantially inferior to our complete FocusDPO formulation. These findings empirically validate the necessity of the integrated masking strategy and confirm the theoretical soundness of our proposed framework.

A.3 Hyperparameter Sensitivity Analysis

We conduct a systematic ablation study to analyze FocusDPO’s sensitivity to two critical hyperparameters that govern the optimization dynamics:

- **Focus Coverage Threshold (τ):** Controls the transition mechanism from purely semantic-guided optimization to the integrated semantic-information density weighting scheme. This parameter determines when adaptive weighting mechanisms are activated during training.
- **Fusion Coefficient (γ):** Modulates the relative contributions between the semantic mask \mathbf{M}_s and the information density mask \mathbf{M}_d in the combined objective function, balancing semantic consistency and detail preservation.

Our hyperparameter sweep evaluates performance across τ and γ values, with validation performance measured using our standard evaluation metrics. The results are visualized in Fig. 10. The empirical analysis reveals optimal convergence at:

- $\tau = 0.1$: Facilitates activation of adaptive weighting at strategically appropriate training phases
- $\gamma = 0.3$: Establishes optimal equilibrium between semantic consistency constraints and information density regularization

Our ablation reveals that FocusDPO exhibits stable performance within reasonable ranges of both hyperparameters, demonstrating the robustness of our approach.

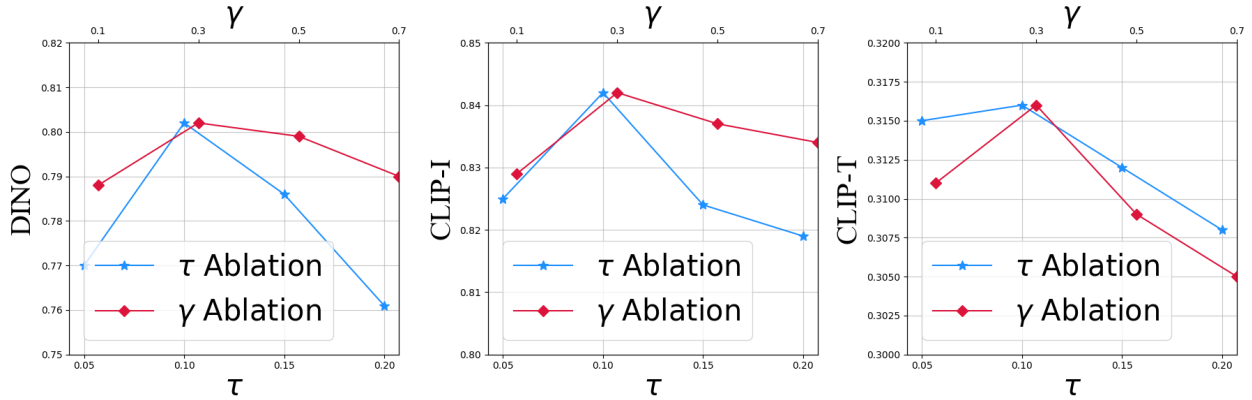


Figure 10 Ablation study on the focus coverage threshold τ and the fusion coefficient γ .

B DIP Dataset Construction and Quality Assurance

B.1 Dataset Overview and Structure

The DIP (Disrupted-Instance Pair Dataset) dataset comprises 10,000 meticulously curated image triplets (x_r, x_0^w, x_0^l) , where x_r denotes the reference image, x_0^w represents the positive (winning) sample, and x_0^l represents the negative (losing) sample. The dataset is systematically organized into two primary configurations:

- **Single-subject subset:** 5,000 triplets focusing on individual subject preservation
- **Multi-subject subset:** 5,000 triplets addressing complex multi-subject scenarios

Each subset maintains balanced representation across three semantic categories: objects, animals, and humans (including real-person and anime styles), ensuring comprehensive coverage of diverse visual domains commonly encountered in personalized generation tasks.

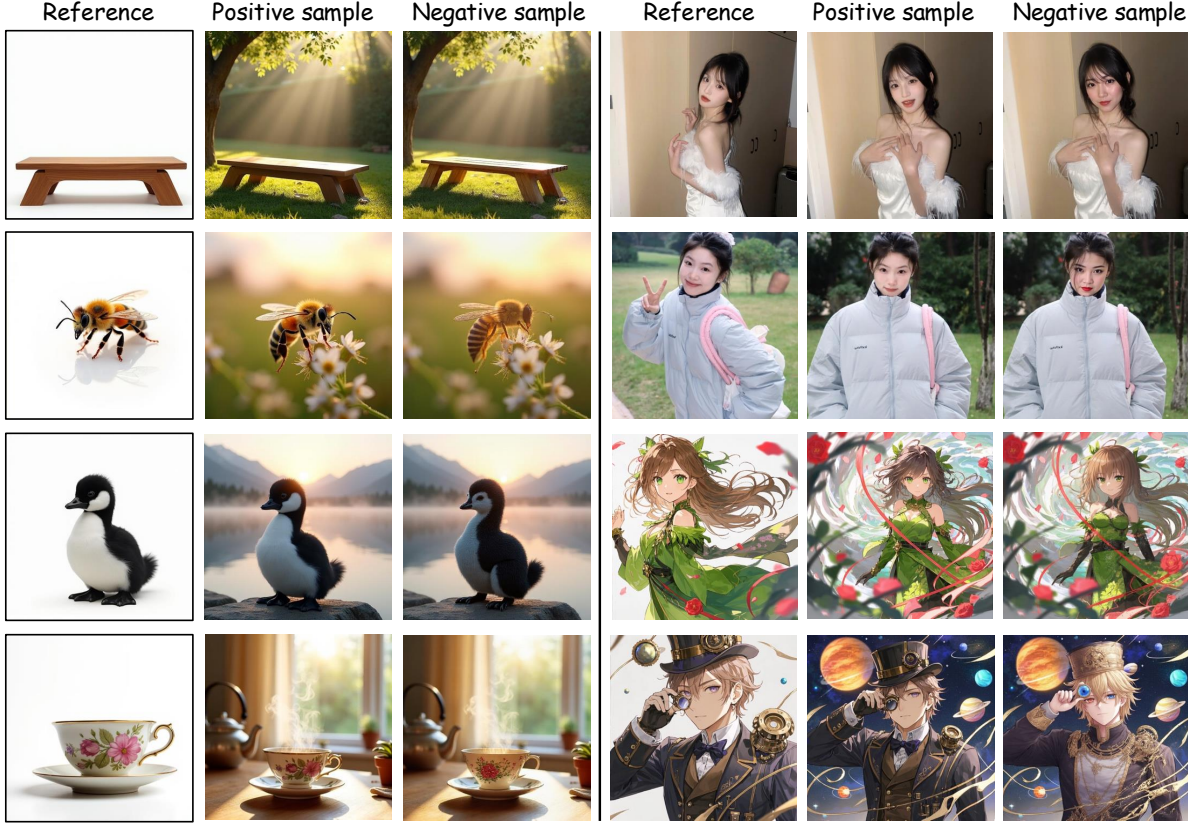


Figure 11 Single-subject examples from the DIP dataset across three content types: object, animal, human.

B.2 Dataset Construction Methodology

Our dataset construction follows a principled two-stage methodology:

Stage 1: Reference-Target Correspondence Establishment We establish semantic correspondences between reference images and positive exemplars, ensuring high-quality alignment across key visual attributes including appearance and contextual elements.

Stage 2: Negative Sample Generation via Instance Disruption We apply systematic perturbation techniques to positive samples, deliberately diminishing subject-reference consistency while maintaining similar compositional structure and prompt descriptions. This approach creates challenging negative examples that share textual similarity with positive samples but exhibit poor visual alignment with references.

A critical insight from our dataset analysis reveals that positive and negative samples often correspond to nearly identical textual prompts, yet exhibit dramatically different levels of reference alignment. **Positive samples demonstrate strong semantic consistency** with preserved key features and subject positioning, while **negative samples show significant deviation** from reference characteristics despite similar descriptive content. This property creates region-aligned positive-negative pairs that provide robust training signals for our FocusDPO framework.

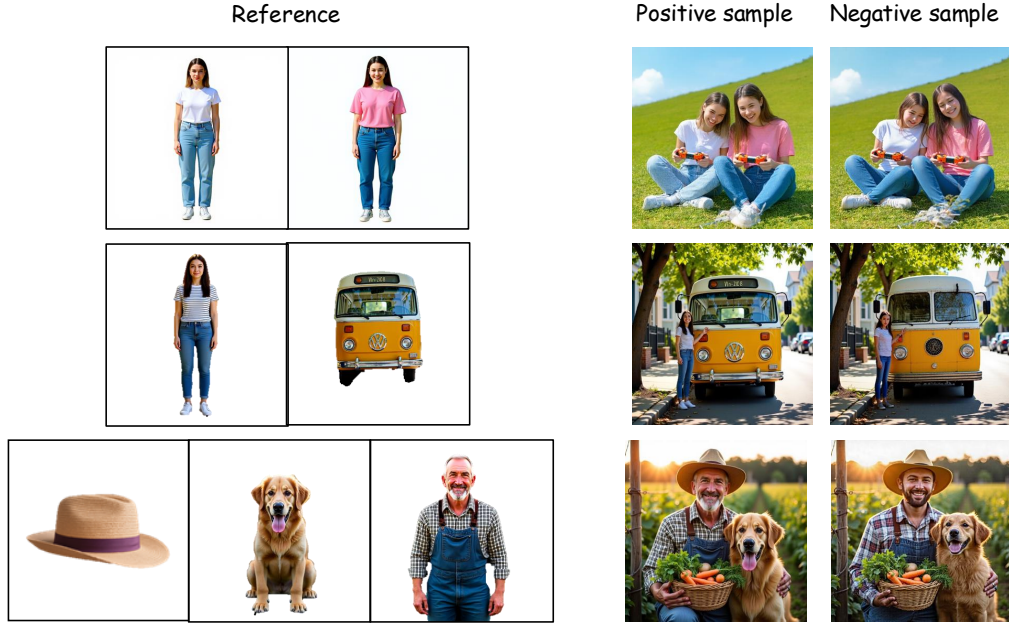


Figure 12 Multi-subject examples from the DIP dataset.

B.3 Quality Assurance Framework

To ensure dataset reliability, we implement a comprehensive dual-validation framework combining automated assessment with expert human annotation:

Automated Evaluation Component: (1) Utilizes GPT-4o as the evaluation engine. (2) Employs ten distinct evaluation queries per semantic category (as shown in Fig. 13). (3) Assesses subject-reference consistency across multiple semantic dimensions. (4) Provides binary responses with scoring based on affirmative classifications.

Manual Annotation Component: (1) Expert annotators with specialized domain knowledge. (2) Standardized evaluation guidelines replicating automated query structure. (3) Consistent 10-point scoring scale across all evaluations. (4) Independent assessment to eliminate potential automated bias.

B.3.1 Consensus-Based Sample Selection

Our sample inclusion criteria require **unanimous agreement** between both evaluation methodologies:

- **Positive samples:** Both GPT-4o and human annotators must assign scores ≥ 9 .
- **Negative samples:** Both evaluation approaches must yield scores ≤ 6 .
- **Ambiguous cases:** Samples with divergent assessments are excluded to ensure dataset purity.

This stringent consensus requirement eliminates borderline cases and ensures that the final DIP dataset comprises only samples with robust consistency classifications, significantly enhancing the reliability of our training framework.

B.4 Dataset Visualization and Analysis

B.4.1 Single-Subject Examples

Fig. 11 presents representative samples from our single-subject configuration, showcasing the diversity across object, animal, and human categories. These examples demonstrate the clear distinction between positive

samples (maintaining strong reference alignment) and negative samples (exhibiting semantic drift while preserving similar compositional structure).

B.4.2 Multi-Subject Examples

Fig. 12 exhibits multi-subject instantiations, highlighting the increased complexity of maintaining consistency across multiple reference subjects. These samples illustrate the dataset’s capability to support training for challenging multi-subject scenarios where existing methods typically fail.

B.4.3 Evaluation Standards

Fig. 13 details our identity consistency evaluation criteria across human, animal, and object categories, providing transparency in our quality assessment methodology and enabling reproducible dataset construction procedures.

Human Identity Consistency Evaluation Criteria
<ol style="list-style-type: none"> 1. **Single Subject**: Does each image contain exactly one human subject (no crowds/obstructions)? 2. **Clothing - Critical Aspects**: Are the styles and patterns of the garments different? 3. **Hair Accessories - Critical Aspects**: Do the number of hair accessories differ? If the difference in quantity is due to occlusion caused by different character movements, return "Yes". 4. **Hairstyle, Color**: Are the hairstyle and hair color identical in both images? 5. **Shoes and Socks**: Are the style and color of shoes, as well as the color and length of socks, identical? If obscured or not visible, return "Yes". 6. **Iris/Pupils**: Are the pupil colors in both images similar? If obscured or not visible, return "Yes". 7. **Facial Features**: Are the features of eyes, nose, and mouth basically the same (ignore the influence of facial expression)? If obscured or not visible, return "Yes". 8. **Clothing**: Are there differences in the garment details including length, cuff style, collar style, and decorative elements such as buttons? 9. **Hair Accessories**: Are the hair characteristics consistent between both images, including hair length, hair accessory size, position, and style? 10. **Additional Accessories - Critical Aspects**: Do the presence or absence of accessories differ? Items held in hands (such as swords, knives, and other props) are not within the scope of evaluation.
Animal Identity Consistency Evaluation Criteria
<ol style="list-style-type: none"> 1. **Single Subject**: Does each image contain exactly one animal subject (no multiple animals/obstructions)? 2. **Species and Breed**: Are the species and breed characteristics identical in both images? 3. **Fur/Coat Pattern**: Are the fur patterns, markings, and colorations consistent between both images? 4. **Body Proportions**: Are the body size, limb proportions, and overall physical structure similar? If partially obscured, return "Yes". 5. **Facial Features**: Are the eye shape, nose/snout characteristics, and ear structure basically the same? If obscured or not visible, return "Yes". 6. **Eye Color**: Are the eye colors similar in both images? If obscured or not visible, return "Yes". 7. **Distinctive Markings**: Are unique identifying marks, spots, stripes, or patches consistent between images? 8. **Tail Characteristics**: Are the tail length, shape, and fur texture identical? If obscured or not visible, return "Yes". 9. **Accessories - Critical Aspects**: Do the presence or absence of collars, tags, or other worn accessories differ? 10. **Overall Appearance**: Are there significant differences in the animal's general appearance that would affect individual identification? Minor pose variations and natural movement should return "Yes".
Object Identity Consistency Evaluation Criteria
<ol style="list-style-type: none"> 1. **Single Object**: Does each image contain exactly one target object (no multiple objects/obstructions)? 2. **Object Type and Category**: Are the object type and category characteristics identical in both images? 3. **Color and Material**: Are the colors, textures, and material properties consistent between both images? 4. **Size and Proportions**: Are the object dimensions, scale, and proportional relationships similar? If partially obscured, return "Yes". 5. **Shape and Structure**: Are the overall form, geometric properties, and structural elements basically the same? If obscured or not visible, return "Yes". 6. **Surface Details**: Are surface patterns, textures, and finish characteristics similar in both images? If obscured or not visible, return "Yes". 7. **Distinctive Features**: Are unique identifying elements, markings, labels, or design details consistent between images? 8. **Component Parts**: Are the visible components, attachments, and sub-elements identical? If obscured or not visible, return "Yes". 9. **Functional Elements - Critical Aspects**: Do the presence or absence of buttons, handles, switches, or other functional components differ? 10. **Overall Appearance**: Are there significant differences in the object's general appearance that would affect individual identification? Minor angle variations and lighting changes should return "Yes".

Figure 13 Identity Consistency Evaluation Criteria of human, animal and object.